Cold Ionospheric Ions in the Magnetic Reconnection Outflow Region

W. Y. Li, M. André, Yu. V. Khotyaintsev, A. Vaivads, S. A. Fuselier, D. B. Graham, S. Toledo-Redondo, B. Lavraud, D. L. Turner, C. Norgren, et al.

▶ **To cite this version:**

W. Y. Li, M. André, Yu. V. Khotyaintsev, A. Vaivads, S. A. Fuselier, et al.. Cold Ionospheric Ions in the Magnetic Reconnection Outflow Region. Journal of Geophysical Research Space Physics, 2017, 122, pp.10,194-10,202. 10.1002/2017JA024287 . insu-03676939

HAL Id: insu-03676939

https://insu.hal.science/insu-03676939

Submitted on 24 May 2022

HAL is a multi-disciplinary open access archive for the deposit and dissemination of scientific research documents, whether they are published or not. The documents may come from teaching and research institutions in France or abroad, or from public or private research centers.

L'archive ouverte pluridisciplinaire **HAL**, est destinée au dépôt et à la diffusion de documents scientifiques de niveau recherche, publiés ou non, émanant des établissements d'enseignement et de recherche français ou étrangers, des laboratoires publics ou privés.

Copyright

AGU PUBLICATIONS

JGR

Journal of Geophysical Research: Space Physics

RESEARCH ARTICLE

10.1002/2017JA024287

Special Section:
Magnetospheric Multiscale (MMS) mission results throughout the first primary mission phase

Cold Ionospheric Ions in the Magnetic Reconnection Outflow Region

W. Y. Li[1], M. André[1], Yu. V. Khotyaintsev[1], A. Vaivads[1], S. A. Fuselier[2], D. B. Graham[1], S. Toledo-Redondo[3], B. Lavraud[4,5], D. L. Turner[6], C. Norgren[1,7], B. B. Tang[8], C. Wang[8], P.-A. Lindqvist[9], D. T. Young[2], M. Chandler[10], B. Giles[11], C. Pollock[12], R. Ergun[13], C. T. Russell[14], R. Torbert[15], T. Moore[11], and J. Burch[2]

[1]Swedish Institute of Space Physics, Uppsala, Sweden, [2]Southwest Research Institute, San Antonio, TX, USA, [3]Science Directorate, European Space Agency, ESAC, Madrid, Spain, [4]Institut de Recherche en Astrophysique et Planétologie, Université de Toulouse (UPA), Toulouse, France, [5]Centre National de la Recherche Scientifique, UMR 5277, Toulouse, France, [6]Space Sciences Department, Aerospace Corporation, El Segundo, CA, USA, [7]Department of Physics and Astronomy, Uppsala University, Uppsala, Sweden, [8]State Key Laboratory of Space Weather, National Space Science Center, Chinese Academy of Sciences, Beijing, China, [9]Space and Plasma Physics, KTH Royal Institute of Technology, Stockholm, Sweden, [10]NASA Marshall Space Flight Center, Huntsville, AL, USA, [11]NASA Goddard Space Flight Center, Greenbelt, MD, USA, [12]Denali Scientific, Healy, AK, USA, [13]Laboratory for Atmospheric and Space Physics, University of Colorado Boulder, Boulder, CO, USA, [14]Earth Planetary and Space Sciences, University of California, Los Angeles, CA, USA, [15]Space Science Center, University of New Hampshire, Durham, NH, USA

Key Points:
- MMS observed cold ionospheric ions deep inside magnetic reconnection outflow
- Cold ion beams are first observed on the magnetosheath edge of ion jet
- Cold ion beams in magnetic reconnection are not Alfvenic in the deHoffman-Teller frame

Supporting Information:
- Figure S1
- Supporting Information S1
- Text S1

Correspondence to:
W. Y. Li,
wyli@irfu.se

Citation:
Li, W. Y., André, M., Khotyaintsev, Y. V., Vaivads, A., Fuselier, S. A., Graham, D. B., … Burch, J. (2017). Cold ionospheric ions in the magnetic reconnection outflow region. *Journal of Geophysical Research: Space Physics*, *122*, 10,194–10,202. https://doi.org/10.1002/2017JA024287

Received 22 APR 2017
Accepted 15 SEP 2017
Accepted article online 20 SEP 2017
Published online 19 OCT 2017

©2017. American Geophysical Union. All Rights Reserved.

Abstract Magnetosheath plasma usually determines properties of asymmetric magnetic reconnection at the subsolar region of Earth's magnetopause. However, cold plasma that originated from the ionosphere can also reach the magnetopause and modify the kinetic physics of asymmetric reconnection. We present a magnetopause crossing with high-density (10–60 cm^{-3}) cold ions and ongoing reconnection from the observation of the Magnetospheric Multiscale (MMS) spacecraft. The magnetopause crossing is estimated to be 300 ion inertial lengths south of the X line. Two distinct ion populations are observed on the magnetosheath edge of the ion jet. One population with high parallel velocities (200–300 km/s) is identified to be cold ion beams, and the other population is the magnetosheath ions. In the deHoffman-Teller frame, the field-aligned magnetosheath ions are Alfvénic and move toward the jet region, while the field-aligned cold ion beams move toward the magnetosheath boundary layer, with much lower speeds. These cold ion beams are suggested to be from the cold ions entering the jet close to the X line. This is the first observation of the cold ionospheric ions in the reconnection outflow region, including the reconnection jet and the magnetosheath boundary layer.

1. Introduction

Low-energy (few eV) ions of ionospheric origin are often present in the magnetosphere (Chappell et al., 1980; Cully et al., 2003; Moore et al., 1997). In the Earth orbit, the spacecraft can be positively charged to several to tens of volts due to the photoelectron emission, preventing the low-energy ions from reaching the spacecraft, and therefore, they cannot be detected. With large-scale convective motion, for example, magnetopause fluctuation, low-energy ions can be accelerated via the $\mathbf{E} \times \mathbf{B}$ drift to overcome the positive spacecraft potential, and be detected by an onboard particle instrument. Besides such direct detection by particle instruments, cold ions can be studied using a technique based on the detection of the wake behind a charged spacecraft in a supersonic ion flow (André et al., 2015; Engwall et al., 2009). Statistics show that low-energy ions dominate the plasma density in large regions of the nightside magnetosphere and polar regions (André & Cully, 2012). At times, the low-energy ions can also dominate in the dayside magnetosphere and can change the dynamics of magnetic reconnection (Fuselier, Burch, et al., 2016).

Magnetic reconnection is a fundamental and universal process to convert energy stored in the magnetic field to kinetic energy of charged particles (Burch, Torbert, et al., 2016; Yamada et al., 2010). The magnetopause is one unique region to investigate reconnection in a collisionless plasma with in situ data, which is important for understanding the solar wind and magnetosphere coupling system (Dungey, 1961). Reconnection at the

magnetopause is typically asymmetric due to the large plasma and magnetic field differences between the magnetosheath and the magnetosphere. The magnetosheath ion and electron gyroradii and inertial lengths determine the two kinetic scales of the diffusion region, namely, ion and electron diffusion regions (Yamada et al., 2010). In the presence of cold ions, a new length scale determined by the cold ion gyroradius is suggested to be in between those of magnetosheath ions and electrons (Divin et al., 2016; Toledo-Redondo et al., 2015, 2016). Besides the modification of reconnection structure, cold ions can reduce the Alfvén speed and the reconnection rate, indicating a localized reduction in the solar wind-magnetosphere coupling (Walsh et al., 2014; Wang et al., 2015). The magnetospheric separatrix layers, which separate the magnetosphere and the reconnection outflow region, are typically characterized by strong currents and normal (Hall) electric fields (Khotyaintsev et al., 2006). When cold ions are present in the magnetospheric separatrix layers, they can remain frozen-in together with electrons and can therefore reduce the Hall currents. This modification of the Hall physics due to cold ions has been studied through investigating the generalized Ohm's law using observations from the Cluster (Toledo-Redondo et al., 2015) and Magnetospheric Multiscale (André et al., 2016) spacecraft. Lower hybrid waves (Graham et al., 2017), ion acoustic waves (Uchino et al., 2017), and electron acoustic waves (Ergun, Holmes, et al., 2016) can be generated at the magnetopause boundary layer due to the interaction of magnetosheath and cold magnetospheric plasmas. Thus, cold ions can affect the magnetic reconnection in both the fluid and kinetic aspects.

He^+ that originated from the ionosphere was detected in the magnetosheath boundary layer (Fuselier et al., 1991; Sonnerup et al., 1981). This observation supports that the magnetospheric cold ions are expected to cross the magnetopause current sheet to the magnetosheath boundary layer along reconnected field lines (Cowley, 1982). Direct detection of cold protons on the magnetosheath side of a reconnection jet has not been reported to our knowledge. Here we investigate a Magnetospheric Multiscale (MMS) magnetopause crossing with high-density cold ions and ongoing magnetic reconnection. He^+ is used to trace the cold ions in the reconnection jet and magnetosheath boundary layer. Cold ion beams (mostly protons) are observed on the magnetosheath edge of the ion jet, and their dynamics are investigated in detail. We report the first observation of the cold ionospheric ions in the reconnection outflow region.

2. Observations

The MMS mission was launched on 13 March 2015 and started the Phase 1A science data collection in September 2015 (Burch, Moore, et al., 2016; Fuselier, Lewis, et al., 2016). We use magnetic field data from the fluxgate magnetometer (FGM) (Russell et al., 2016) and electric field from the electric double probe (EDP) (Ergun, Tucker, et al., 2016; Lindqvist et al., 2016). The particle data are from the Fast Plasma Investigation (FPI) (Pollock et al., 2016) sampled at 4.5 s (fast mode) and 0.15 s for ions and 0.03 s for electrons (burst mode), the mass-resolved instrument Hot Plasma Composition Analyzer (HPCA) (Young et al., 2016) and the Fly's Eye Energetic Particle Spectrometer (FEEPS) instrument (Blake et al., 2016) for energetic electron data at 0.3 s resolution. We investigate a magnetopause crossing observed between 03:12 and 03:44 UT on 1 November 2015. During the spacecraft transition from the magnetosphere to the magnetosheath, the solar wind conditions were quasi-steady, and the interplanetary magnetic field (IMF), [−4.6, 7.0, 0.0] nT, was close to the Parker spiral orientation (Parker, 1965). The MMS spacecraft were located at [9.3, 1.4, −0.3] R_E (GSE) during this time interval, and were in a tetrahedron formation with 10–15 km separation.

An overview is presented in Figure 1: Shown from top to bottom are (a) magnetic field, (b) ion and electron number densities from FPI and electron number density derived from the Langmuir wave observations from EDP. (c) Ion bulk velocity, (d) ion, and (e) electron omnidirectional differential energy fluxes. (f) Spacecraft potential and (g) electric field. The vectors are presented in the Geocentric Solar Ecliptic (GSE) coordinate system, unless otherwise stated. We identify the magnetosphere by high-energy (several keV) ions and electrons, nearly stagnant plasma bulk velocity, and predominantly northward magnetic field. The magnetosheath is characterized by intermediate energy ions (100–1,000 eV) and electrons (50–100 eV) and predominantly duskward magnetic field (B_Y). The magnetosheath ion speed is about 50 km/s, mostly along the Y direction (Figure 1c). This low speed is consistent with the spacecraft location near the subsolar region. Several ion fast flows were observed by MMS from 03:19 to 03:41 UT due to the several partial crossings with multiple encounters of the separatrix region. The strongest flow between 03:30 and 03:31 UT has $V_Y \sim 300$ km/s and $V_Z \sim -200$ km/s. The magnitudes of the fast ion flows are consistent with the jet speeds of asymmetric reconnection at the magnetopause (Cassak & Shay, 2007). These jets indicate ongoing reconnection between

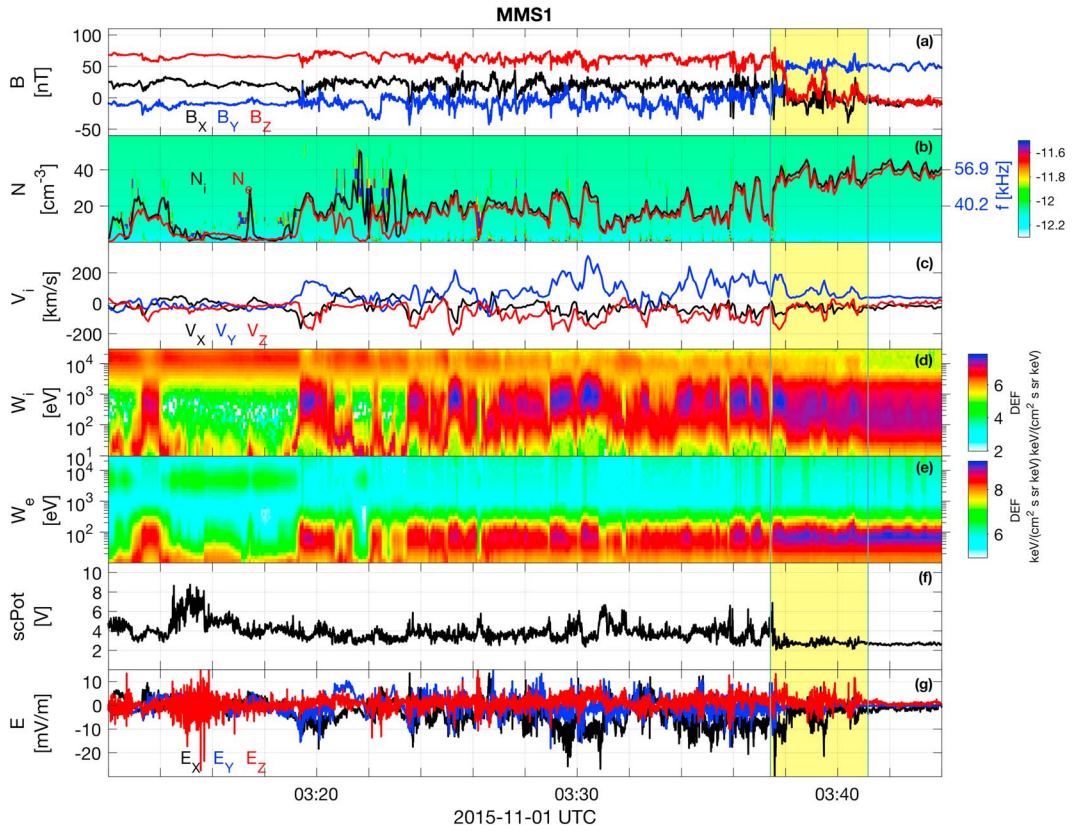

Figure 1. MMS observation of the magnetopause crossing on 1 November 2015. MMS1 data of (a) magnetic field, (b) number densities of ions N_i and electrons N_e from FPI and electron density derived from the Langmuir wave observations from EDP, (c) ion bulk velocity $\mathbf{V}_i$, (d) ion and (e) electron omnidirectional differential energy fluxes, (f) spacecraft potential, and (g) electric field. The FPI data are in the fast mode. The spectrogram in Figure 1b shows the power spectral density ($V^2/m^2/Hz$) of electric field from the EDP instrument, and the Langmuir frequency ($f = 1/(2\pi)\sqrt{N_e e^2/m_e \epsilon_0}$) is indicated by the strong wave activity. Here m_e is the mass of electron, and ϵ_0 is the permittivity in vacuum. The yellow-shaded region indicates a complete magnetopause crossing from the magnetosphere to the magnetosheath.

northward (magnetospheric) and duskward (magnetosheath) magnetic fields, and the jet directions indicate that the spacecraft were located south of the reconnection X line.

As shown in Figure 1d, cold ions, with ~10 eV thermal energy, are present in the magnetosphere, while their total energy can reach 100 eV due to the $\mathbf{E} \times \mathbf{B}$ drift. The cold ion density from the burst-mode FPI data varies from 10 to 60 cm^{-3} through the entire interval. The lowest-energy channel of the FPI ion detector is about 10 eV, and the spacecraft potential in the magnetosphere is about 4 V on average. The large variances in the cold ion density can be due to FPI missing a part of the cold ion population because of its low energy and the positive spacecraft potential, as well as due to the actual variance of the cold ion density. Sometimes, for example, around 03:20:10 UT, the electron density is underestimated compared with the ion density, while the ion density is consistent with the plasma density estimated from the waves at the electron plasma frequency. This underestimation is because a large portion of the electrons with low thermal energy are not detected by FPI.

The yellow-shaded region in Figure 1 highlights the only complete crossing from the magnetosphere to the magnetosheath, and the magnetopause current sheet with the rotation of the magnetic field occurs around 03:38 UT. Figure 2 presents a detailed plot of the complete magnetopause crossing from 03:37:25 to 03:41:10 UT. At the beginning of this interval, MMS were located in the magnetosphere. The cold ions in the magnetosphere have pitch angles predominantly perpendicular to the magnetic field (Figure 2h). The magnetospheric separatrix crossing at 03:37:30 UT (the first black line in Figure 2) is identified by the increase in plasma density, partial loss of magnetospheric high-energy electrons (Figure 2d) and Hall electric field (not shown). Around 03:38:00 UT, MMS crossed the magnetopause current sheet from the ion jet to the

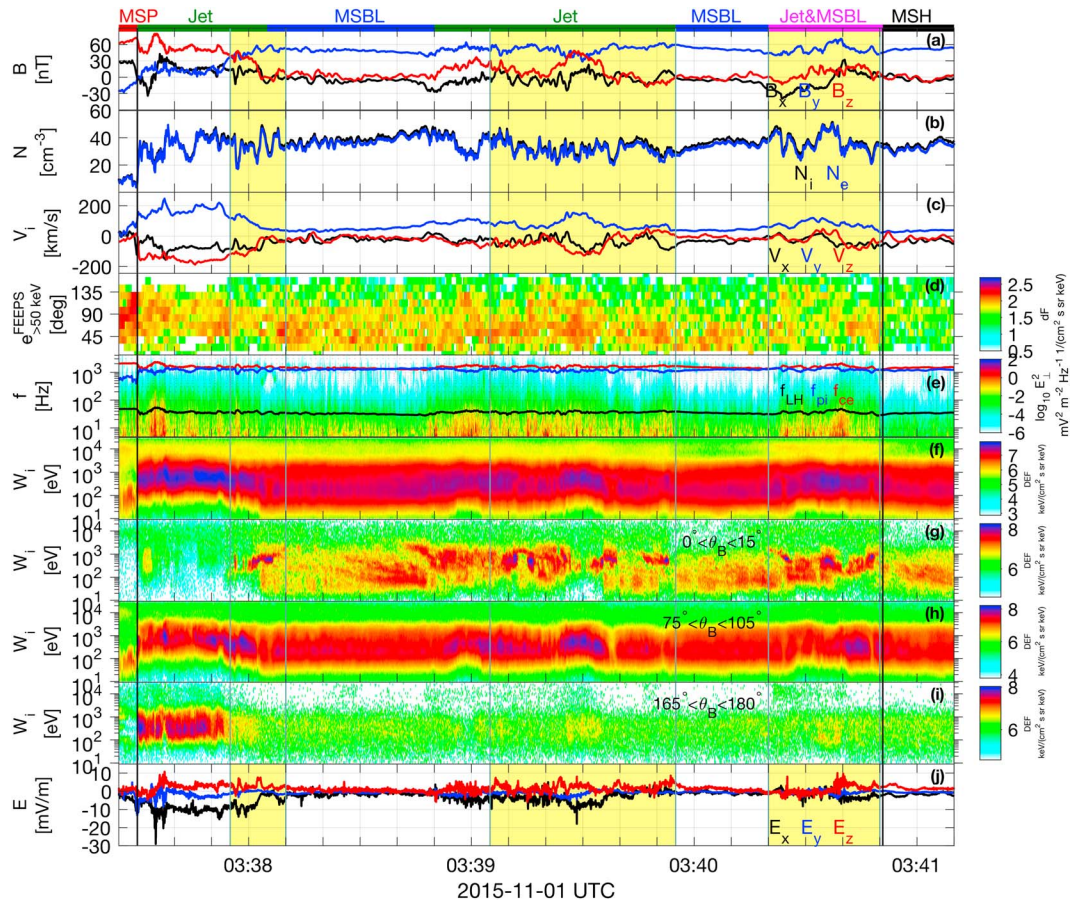

Figure 2. Magnetopause crossing from the magnetosphere to magnetosheath by MMS1. From top to bottom, (a) magnetic field; (b) ion and electron number densities; (c) ion bulk velocity; (d) pitch angle distributions of energetic (50–500 keV) electrons from FEEPS; (e) spectrogram of perpendicular E fluctuation with lower hybrid (black), ion plasma (blue), and electron cyclotron (red) frequencies. Ion (f) omnidirectional, (g) parallel, (h) perpendicular, and (i) antiparallel differential energy fluxes in the spacecraft frame; and (j) electric field. The thick bars at the top of Figure 2a denote magnetosphere (MSP, red), reconnection jet (green), magnetosheath boundary layer (MSBL, blue), and magnetosheath (MSH, black). The magenta bar denotes a mixed region with the jet and magnetosheath boundary layer. Two vertical black lines represent magnetospheric and magnetosheath separatrices, respectively. Three yellow-shaded intervals indicate regions with cold ion beams in reconnection. The FPI data are in the burst mode.

magnetosheath boundary layer, and the current sheet is characterized by the magnetic field rotating from northward to duskward and a decrease in the southward outflow speed. The features distinguishing the magnetosheath boundary layer from the magnetosheath are magnetospheric high-energy electrons (Figure 2d) and stronger wave fluctuations (Figure 2e). From 03:39:05 to 03:39:55 UT, MMS moved back to the jet region with increases in B_Z and V_i. From 03:39:55 to 03:40:20 UT, MMS were located in the magnetosheath boundary layer again. The magnetosheath separatrix separates the magnetosheath and reconnected magnetic field lines. The MMS crossing of the magnetosheath separatrix at 03:40:50.8 UT (the second black line in Figure 2) is identified by a sharp boundary in the power spectral density of the electric field (Figure 2e) and a decrease in the high-energy electrons of the magnetospheric origin (Figure 2d). Before the magnetosheath separatrix crossing, B_Z and V_i increased slightly between 03:40:20 and 03:40:50 UT. We interpret this interval as a mixed region of the ion jet and magnetosheath boundary layer.

We perform minimum variance analysis (MVA) (Paschmann & Daly, 1998) on the magnetic field measurements between 03:37:47 and 03:38:15 UT, which yields the maximum (**L** = [0.27, −0.59, 0.76]), intermediate (**M** = [−0.28, −0.80, −0.53]), and minimum (**N** = [0.92, −0.07, −0.38]) variance directions. Multispacecraft timing analysis (Paschmann & Daly, 1998) of B_Z around 03:38:03 UT results in a boundary velocity of $\mathbf{V}_N = 53 \times [-0.98, 0.10, 0.15]$ km/s (GSE), which is consistent with the normal direction from MVA method. The normal velocity of the first jet region is about 50 km/s on average. Based on this, the width of the jet in the normal

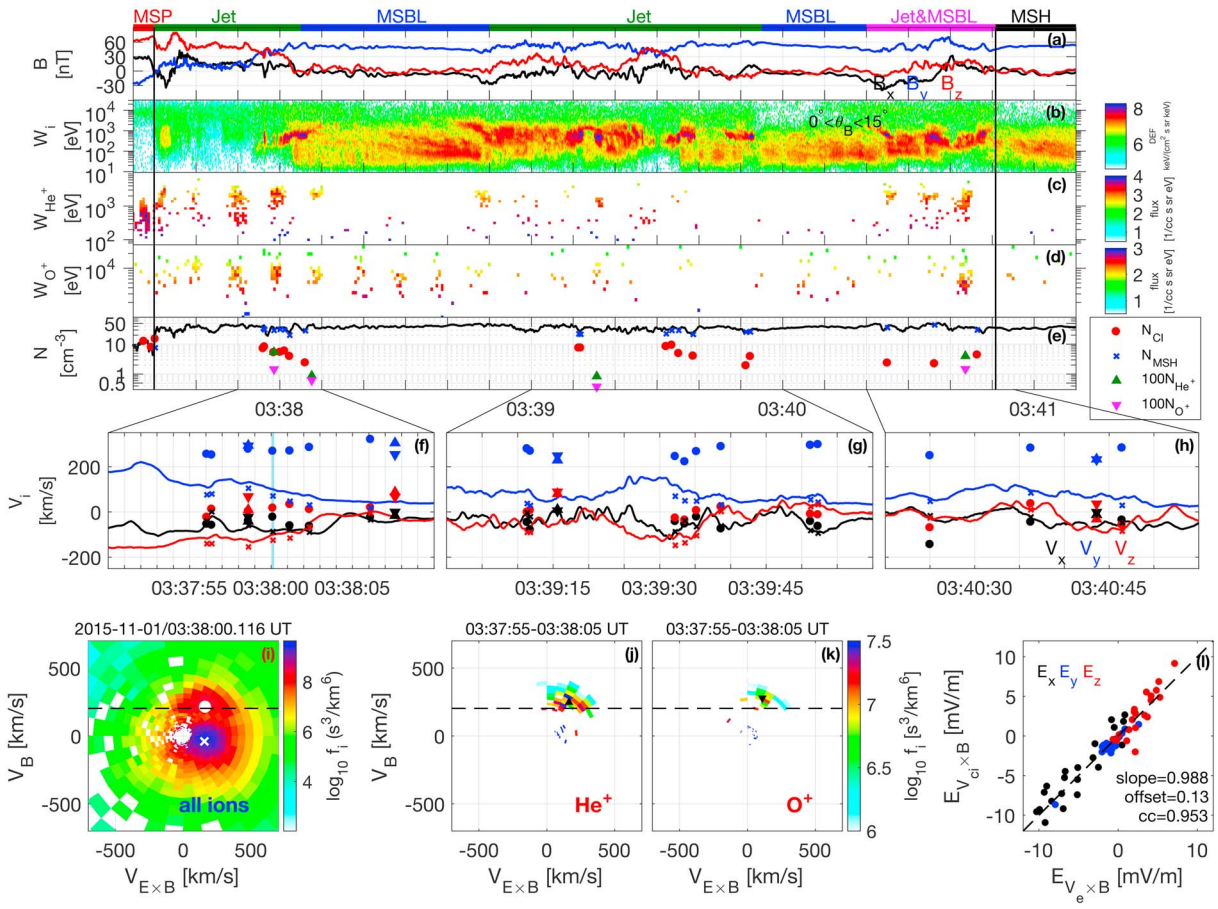

Figure 3. Cold ion beams from the FPI and HPCA measurements. From top to bottom, (a) magnetic field; (b) ion parallel differential energy flux in the spacecraft frame; (c) He^+ and (d) O^+ differential particle fluxes in the spacecraft frame; (e) number densities; and (f–h) bulk velocities of FPI ion (curve), cold ion (circle), magnetosheath ion (cross), He^+ (upward triangle), and O^+ (downward triangle). The number densities of He^+ and O^+ in Figure 3e are multiplied by 100. (i) Ion 2-D distribution function in the spacecraft frame to show an example of the frozen-in MSH ions and cold ion beam, with cross and circle denoting the individual bulk velocities. (j) He^+ and (k) O^+ 2-D plots of distribution functions in the spacecraft frame from HPCA between 03:37:55 and 03:38:05 UT. HPCA provides complete distribution functions of different ion species at half-spin resolution (~10 s). and the dashed lines indicate $V_B = V_A$. (l) Scatterplot of cold ion and electron convection electric fields to verify the calculation of partial moments.

direction is estimated to be about 50 d_i, where the ion inertial length d_i = 36 km is based on the magnetosheath ion number density (40.3 cm^{-3}). We assume that the angle between the magnetospheric separatrix and the magnetopause current sheet is about 10° (Pritchett, 2008), which indicates that the MMS magnetopause crossing is far (300 d_i or shorter) away from the X line. Timing analysis on the magnetic field and density data of the boundaries within 03:38:45–03:41:00 UT supports the interpretation of back-and-forth crossings of the jet and the magnetosheath boundary layer. Figures 2g–2i present the parallel, perpendicular, and antiparallel ion differential energy fluxes in the spacecraft frame. Intense ion fluxes near 500 eV appear along the parallel direction in the three yellow-shaded regions, which are located on the magnetosheath edge of the ion jet. We focus on these intense parallel ion fluxes and identify them to be cold ion beams from the cold ion inflow on the magnetospheric side.

We use the minor species to get the origins of the ion populations in the reconnection outflow region. There are three main contributors to plasma density on the magnetospheric side: the plasmaspheric drainage plume, the warm plasma cloak, and the ring current. The three sources can be distinguished by their energies and composition (Fuselier, Burch, et al., 2016). We observe cold He^+ together with cold protons in the magnetosphere, with negligible low-energy O^+. This suggests that the plasmaspheric drainage plume is the source of the cold H^+ and He^+ in this event. A small population of O^+ with energy from several to tens of keV was detected in the magnetosphere, the ion jet, and the magnetosheath boundary layer, and the source of these high-energy O^+ is likely to be the warm plasma cloak and/or the ring current. The minor ion species

in the magnetosheath is mostly He^{++} from solar wind (not shown). Therefore, we use He^{+} as a tracer of cold magnetospheric ions to investigate their existence and dynamics in the reconnection outflow region.

Figure 3i presents an example of an ion distribution function in the $\mathbf{V}_{\mathbf{E}\times\mathbf{B}}$ and $\mathbf{V}_{\mathbf{B}}$ plane, which shows existence of two ion populations. The two populations share the same $\mathbf{E}\times\mathbf{B}$ drift velocity. The hotter population has a low negative $\mathbf{V}_{\mathbf{B}}(\sim -40$ km/s), while the colder population has $\mathbf{V}_{\mathbf{B}} \sim 210$ km/s, which is close to the local Alfvén velocity. The parallel temperatures of the cold and the hot ions are 55 eV and 81 eV, respectively, and their perpendicular temperatures are 108 eV and 148 eV. The cold parallel population in Figure 3i is representative of the parallel ion populations in Figure 3b, with lower temperatures than those of the other ion populations and the magnetosheath ions. He^{+} shows similar parallel distributions from the complete distribution function obtained between 03:37:55 and 03:38:05 UT (Figure 3j), which confirms that the intense parallel ion fluxes shown in Figure 3b are the ion beams originating from the cold ion inflow on the magnetospheric side. Meanwhile, O^{+} has a similar parallel distribution in Figure 3k. From 03:38:15 to 03:38:45 UT, three complete distribution functions of O^{+} were measured, while cold ion beam was not observed by FPI or HPCA. This further supports that O^{+} came from a different magnetospheric source than the cold ions.

To study the dynamics of the cold ion beams, we separate each investigated FPI ion distribution function into cold magnetospheric, magnetosheath, and hot magnetospheric distribution functions when the first two populations are distinct from each other (see Figure S1 in the supporting information for more details), and compute their partial moments, including number density (Figure 3e), bulk velocity (Figures 3f–3h), and parallel and perpendicular temperatures. The results of He^{+} and O^{+} are also included in these panels. The number densities of the cold ion beams vary between 2 and 10 cm^{-3}, while the magnetosheath density is about 30 cm^{-3}. In the three intervals of Figures 3f–3h, the bulk velocity of magnetosheath ions is close to the average velocity from the FPI data, and both velocities are predominantly perpendicular to **B**. The cold ion beams have the same perpendicular velocities and much higher parallel velocities (200 to 300 km/s). In Figure 3l, the comparison between the electron and cold ion convection electric fields demonstrates good reliability of the partial moment calculation from the FPI distribution functions. The standard deviation of the difference between the two convection electric fields is about 2 mV/m, which indicates about 30 km/s error in the cold ion perpendicular velocity; the error in the parallel velocity is assumed to be on the same level.

3. Discussion

The magnetopause during ongoing steady reconnection at a thin current sheet is believed to be a rotational discontinuity (RD) (Sonnerup et al. 1981). Across an RD, a proper frame of reference, namely the deHoffman-Teller (HT) frame, can be found in which the electric field vanishes on both sides of the discontinuity. The ion bulk flow in the HT frame is Alfvénic on both sides of a rotational discontinuity based on single-fluid magnetohydrodynamics (MHD) theory (Hudson, 1970; Sonnerup et al. 1981). Cowley (1982) provided a kinetic description of multifluid plasma crossing a rotational discontinuity both from the magnetosheath and the magnetosphere and suggested that the speeds of field-aligned ions do not change when ions from each side are transmitted or reflected across the current sheet. Using in situ plasma composition measurements, Fuselier et al. (1991) showed that He^{+} flow from the magnetosphere on the magnetosheath side of a current sheet and He^{++} flow from the magnetosheath on the magnetospheric side are both field-aligned and Alfvénic in the HT frame.

We perform the Walén analysis (Paschmann & Daly, 1998) on this MMS event to examine the cold proton flows across the magnetopause current sheet. The HT analysis is performed on the three intervals of Figures 3f–3h, and proper HT velocities with the slope ~1 and correlation coefficient ~1 are found for the first two intervals, and not for the third one. Figures 4a and 4b present the HT analysis of the first two intervals in the LMN coordinate system. The two similar HT velocities are close to the Alfvén velocities in the magnetosheath boundary layer, which is consistent with previous studies (e.g., Fuselier et al., 1991). We perform the Walén test on the first two intervals in the average $\mathbf{V}_{HT}$ frame, as shown in Figure 4c. The Alfvén velocity is estimated from the magnetic field and FPI ion number density, assuming that all ions are protons. The number densities of He^{+} and O^{+} are about two magnitudes smaller than those of the protons (Figure 3e), and their populations do not affect the Alfvén velocity estimated from the proton mass density. The gray dots indicate the field-aligned ion flow directly from FPI. The crosses and circles indicate magnetosheath and cold ions from the partial moment calculation, respectively. The negative slope of the dots and crosses are consistent with the magnetopause current sheet crossing south of the X line. The slope magnitude (0.93) of the crosses indicates that the field-aligned

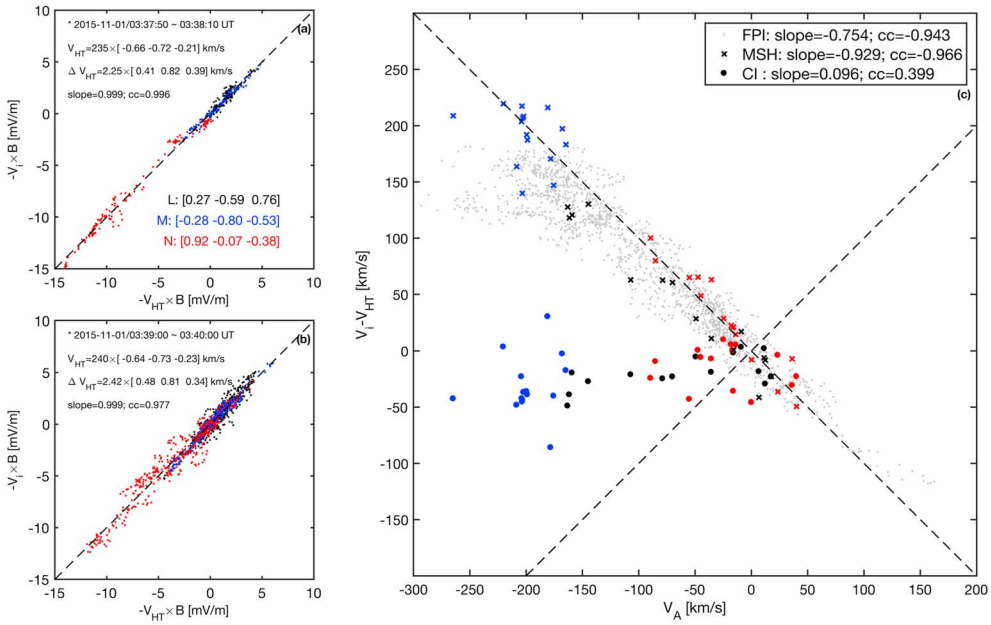

Figure 4. Walén test of the magnetosheath ions and cold ion beams in the LMN coordinate system. (a, b) Scatterplot of ion convection electric fields versus $-\mathbf{V}_{HT} \times \mathbf{B}$ of the intervals of Figures 3f and 3g. The two intervals have similar deHoffman-Teller velocities. (c) Scatterplot of ion velocities in the HT frame versus the Alfvén velocity. The circles and crosses denote cold ion beams and magnetosheath ions, respectively.

magnetosheath ions are nearly Alfvénic. It is larger than the slope magnitude (0.75) of the FPI data, while the FPI velocities are the average between the magnetosheath ions and cold ion beams. Retinò et al. (2005) showed a similar improvement when performing the Walén test only on the transmitted magnetosheath ion populations across the magnetopause current sheet. In the HT frame, the field-aligned magnetosheath ions move toward the jet region, and the field-aligned cold ion beams move toward the magnetosheath boundary layer at V ~ 50 km/s (0.18 of the local Alfvén speed). The He^+ and O^+ flows in the HT frame are not Alfvénic, confirming that they follow similar processes as H^+.

The cold ion beams are minor populations and contribute a small portion of the pressure balance in the Rankine-Hugoniot conditions across a rotational discontinuity (Hudson, 1970). Therefore, the field-aligned cold ion beams are not required to be Alfvénic in the HT frame. After the crossing of the magnetospheric separatrix at 03:37:30 UT shown in Figure 3, cold ions are indistinguishable from the magnetosheath ions in the FPI velocity distribution functions until the magnetosheath edge of the jet. During the interval from 03:37:30 to 03:37:55 UT, three complete distribution functions of He^+ and O^+ are measured by HPCA. This demonstrates that a large population of cold ions exists in the ion jet. These cold ions are heated, accelerated, and mixed with the magnetosheath ions through the pickup process (Drake et al., 2009; Wang et al., 2014). In the HT frame, the picked-up cold ions move together with the magnetosheath ions along the antiparallel direction. No cold ion beams along the parallel direction are observed by MMS inside the jet (e.g., 03:37:30 to 03:37:55 UT). The black arrow-headed curve with red dots in Figure 5 denotes the picked-up cold ions from the cold ion inflow entering the jet far from the X line.

We suggest that the parallel cold ion beams on the magnetosheath edge of the jet are from the cold ion inflows near the X line, where the new reconnected field lines and magnetosheath ions have not been fully accelerated by energy release around the X line. The transmitted cold ions are located close to the magnetopause current sheet and pick up a low parallel velocity in the field line (HT) frame. After that, the frozen-in cold ions are accelerated together with the reconnected field lines to a high HT velocity. In the HT frame, the cold ions with a low parallel velocity move toward the magnetosheath side of the jet. In the spacecraft frame, these cold ions have much higher parallel velocities than the local magnetosheath ions. The red arrow-headed curve with black dots in Figure 5 denotes the cold ion beams from the cold ion inflow entering the outflow region close to the X line. Different dynamics of the magnetosheath and cold ions demonstrate different paths of the ion inflows on both sides through the magnetic reconnection. The cold ion outflows, including the

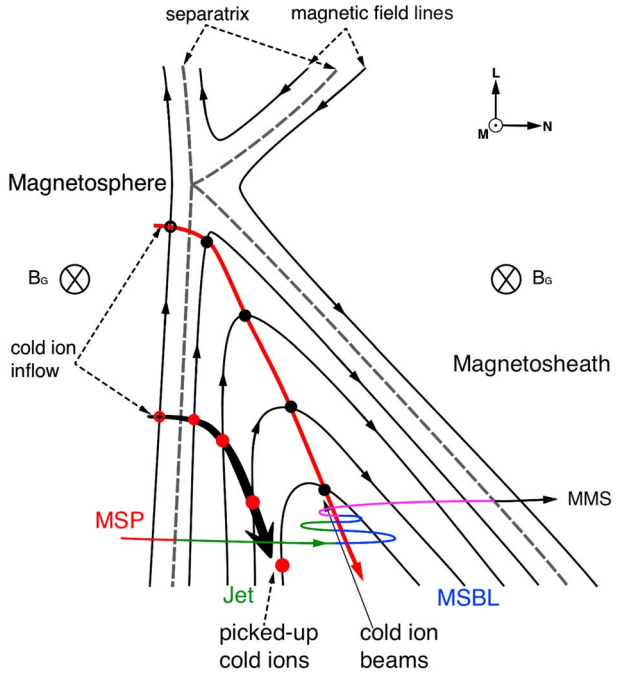

Figure 5. Sketch showing the cold ion outflows in the reconnection region and the MMS trajectory. Two thick curves with arrows denote paths of two cold ion inflows in the reconnection outflow region. The black dots on the red curve indicate cold ion beams, while the red dots on the black curve indicate picked-up cold ions. One colored curve in the bottom part represents the MMS trajectory from the magnetosphere to the magnetosheath, and the same colors are used as in Figure 2.

picked-up cold ions and the cold ion beams, demonstrate that the cold ion inflows close to and far from the X line experience different kinetic processes.

4. Conclusions

We investigate an MMS magnetopause crossing on 1 November 2015 with high-density (10–60 cm^{-3}) cold ions and ongoing reconnection and present the first observation of the cold ionospheric ion outflows throughout the entire reconnection region, including the ion jet and the magnetosheath boundary layer. MMS crossed the magnetopause current sheet far (~300 ion inertial lengths) from the reconnection X line. Two separate ion populations are found in FPI distribution functions measured on the magnetosheath edge of the ion jet. One population with high parallel velocities are identified to be cold ion beams that originated from the ionosphere. The other population with low antiparallel velocities are the magnetosheath ions. Both ion flows are frozen-in with the magnetic fields. The moments of the cold ion beams and the magnetosheath ions are computed by separating velocity space into different regions. He^+, as a minor species of cold plasma, is used as a tracer to identify the presence of cold ions in the reconnection ion jet and the magnetosheath boundary layer. We perform the Walén analysis on the magnetopause current sheet crossing with the cold ion beams. In the HT frame, the field-aligned magnetosheath ions are Alfvénic and move toward the jet region, while the field-aligned cold ion beams move toward the magnetosheath boundary layer, with much lower speeds. These cold ion beams contribute a minor portion of the pressure balance across the magnetopause current sheet (a rotational discontinuity), and therefore can be non-Alfvénic in the HT frame. Cold ionospheric ions entering the jet on the magnetospheric side far from the X line are quickly heated and accelerated by the jet. We suggest that cold ionospheric ions entering the jet close to the X line is the source of the cold ion beams observed on the magnetosheath edge of the jet.

Acknowledgments
The OMNI data were generated by J. H. King and N. Papitashivilli and provided via http://cdaweb.gsfc.nasa.gov/. MMS observations are publicly available via NASA resources and the Science Data Center at CU/LASP (https://lasp.colorado.edu/mms/sdc/public/). This work was supported by Swedish National Space Board (SNSB) contracts 158/16, 176/15, and 67/16. Research at Southwest Research Institute was supported under contract with NASA. W. Y. Li thanks Qinghe Zhang from the School of Space Science and Physics, Shandong University, Weihai, China for checking the plume inside the magnetopause by using TEC data.

References

André, M., & Cully, C. M. (2012). Low-energy ions: A previously hidden solar system particle population. *Geophysical Research Letters*, *39*, L03101. https://doi.org/10.1029/2011GL050242

André, M., Li, K., & Eriksson, A. I. (2015). Outflow of low-energy ions and the solar cycle. *Journal of Geophysical Research: Space Physics*, *120*, 1072–1085. https://doi.org/10.1002/2014JA020714

André, M., Li, W., Toledo-Redondo, S., Khotyaintsev, Y. V., Vaivads, A., Graham, D. B., … Saito, Y. (2016). Magnetic reconnection and modification of the Hall physics due to cold ions at the magnetopause. *Geophysical Research Letters*, *43*, 6705–6712. https://doi.org/10.1002/2016GL069665

Blake, J. B., Mauk, B. H., Baker, D. N., Carranza, P., Clemmons, J. H., Craft, J., … Westlake, J. (2016). The fly's eye energetic particle spectrometer (FEEPS) sensors for the Magnetospheric Multiscale (MMS) mission. *Space Science Reviews*, *199*(1–4), 309–329. https://doi.org/10.1007/s11214-015-0163-x

Burch, J. L., Moore, T. E., Torbert, R. B., & Giles, B. L. (2016). Magnetospheric multiscale overview and science objectives. *Space Science Reviews*, *199*(1), 5–21. https://doi.org/10.1007/s11214-015-0164-9

Burch, J. L., Torbert, R. B., Phan, T. D., Chen, L.-J., Moore, T. E., Ergun, R. E., … Chandler, M. (2016). Electron-scale measurements of magnetic reconnection in space. *Science*, *352*, 6,290. https://doi.org/10.1126/science.aaf2939

Cassak, P. A., & Shay, M. A. (2007). Scaling of asymmetric magnetic reconnection: General theory and collisional simulations. *Physics of Plasmas*, *14*(10), 102,114. https://doi.org/10.1063/1.2795630

Chappell, C. R., Baugher, C. R., & Horwitz, J. L. (1980). New advances in thermal plasma research. *Reviews of Geophysics*, *18*(4), 853–861. https://doi.org/10.1029/RG018i004p00853

Cowley, S. W. H. (1982). The causes of convection in the Earth's magnetosphere: A review of developments during the IMS. *Reviews of Geophysics*, *20*(3), 531–565. https://doi.org/10.1029/RG020i003p00531

Cully, C. M., Donovan, E. F., Yau, A. W., & Arkos, G. G. (2003). Akebono/Suprathermal mass spectrometer observations of low-energy ion outflow: Dependence on magnetic activity and solar wind conditions. *Journal of Geophysical Research*, *108*(A2), 1093. https://doi.org/10.1029/2001JA009200

Divin, A., Khotyaintsev, Y. V., Vaivads, A., André, M., Toledo-Redondo, S., Markidis, S., & Lapenta, G. (2016). Three-scale structure of diffusion region in the presence of cold ions. *Journal of Geophysical Research: Space Physics*, *121*, 12,001–12,013. https://doi.org/10.1002/2016JA023606

Drake, J. F., Swisdak, M., Phan, T. D., Cassak, P. A., Shay, M. A., Lepri, S. T., … Zurbuchen, T. H. (2009). Ion heating resulting from pickup in magnetic reconnection exhausts. *Journal of Geophysical Research*, *114*, A05111. https://doi.org/10.1029/2008JA013701

Dungey, J. W. (1961). Interplanetary magnetic field and auroral zones. *Physical Review Letters*, *6*(2), 47–48. https://doi.org/10.1103/PhysRevLett.6.47

Engwall, E., Eriksson, A. I., Cully, C. M., André, M., Torbert, R., & Vaith, H. (2009). Earth's ionospheric outflow dominated by hidden cold plasma. *Nature Geoscience*, *2*(1), 24–27. https://doi.org/10.1038/ngeo387

Ergun, R. E., Holmes, J. C., Goodrich, K. A., Wilder, F. D., Stawarz, J. E., Eriksson, S., … André, M. (2016). Magnetospheric multiscale observations of large-amplitude, parallel, electrostatic waves associated with magnetic reconnection at the magnetopause. *Geophysical Research Letters*, *43*, 5626–5634. https://doi.org/10.1002/2016GL068992

Ergun, R. E., Tucker, S., Westfall, J., Goodrich, K. A., Malaspina, D. M., Summers, D., … Cully, C. M. (2016). The axial double probe and fields signal processing for the MMS mission. *Space Science Reviews*, *199*(1–4), 167–188. https://doi.org/10.1007/s11214-014-0115-x

Fuselier, S. A., Klumpar, D. M., & Shelley, E. G. (1991). Ion reflection and transmission during reconnection at the Earth's subsolar magnetopause. *Geophysical Research Letters*, *18*(2), 139–142. https://doi.org/10.1029/90GL02676

Fuselier, S. A., Burch, J. L., Cassak, P. A., Goldstein, J., Gomez, R. G., Goodrich, K., … Valek, P. (2016). Magnetospheric ion influence on magnetic reconnection at the duskside magnetopause. *Geophysical Research Letters*, *43*, 1435–1442. https://doi.org/10.1002/2015GL067358

Fuselier, S. A., Lewis, W. S., Schiff, C., Ergun, R., Burch, J. L., Petrinec, S. M., & Trattner, K. J. (2016). Magnetospheric multiscale science mission profile and operations. *Space Science Reviews*, *199*(1), 77–103. https://doi.org/10.1007/s11214-014-0087-x

Graham, D. B., Khotyaintsev, Y. V., Norgren, C., Vaivads, A., André, M., Toledo-Redondo, S., … Burch, J. L. (2017). Lower hybrid waves in the ion diffusion and magnetospheric inflow regions. *Journal of Geophysical Research: Space Physics*, *122*, 517–533. https://doi.org/10.1002/2016JA023572

Hudson, P. D. (1970). Discontinuities in an anisotropic plasma and their identification in the solar wind. *Planetary and Space Science*, *18*(11), 1611–1622. https://doi.org/10.1016/0032-0633(70)90036-X

Khotyaintsev, Y. V., Vaivads, A., Retinò, A., André, M., Owen, C. J., & Nilsson, H. (2006). Formation of inner structure of a reconnection separatrix region. *Physical Review Letters*, *97*, 205,003. https://doi.org/10.1103/PhysRevLett.97.205003

Lindqvist, P.-A., Olsson, G., Torbert, R. B., King, B., Granoff, M., Rau, D., … Tucker, S. (2016). The spin-plane double probe electric field instrument for MMS. *Space Science Reviews*, *199*(1–4), 137–165. https://doi.org/10.1007/s11214-014-0116-9

Moore, T. E., Chappell, C. R., Chandler, M. O., Craven, P. D., Giles, B. L., Pollock, C. J., … Mozer, F. S. (1997). High-altitude observations of the polar wind. *Science*, *277*(5,324), 349–351. https://doi.org/10.1126/science.277.5324.349

Parker, E. N. (1965). Dynamical theory of the solar wind. *Space Science Reviews*, *4*(5), 666–708. http: //dx.doi.org/10.1007/bf00216273

Paschmann, G., & Daly, P. W. (1998). *Analysis Methods for Multi-Spacecraft Data, Noordwijk*. Netherlands: ESA Publications Division.

Pollock, C., Moore, T., Jacques, A., Burch, J., Gliese, U., Saito, Y., … Zeuch, M. (2016). Fast plasma investigation for magnetospheric multiscale. *Space Science Reviews*, *199*(1–4), 331–406. https://doi.org/10.1007/s11214-016-0245-4

Pritchett, P. L. (2008). Collisionless magnetic reconnection in an asymmetric current sheet. *Journal of Geophysical Research*, *113*, A06210. https://doi.org/10.1029/2007JA012930

Retinò, A., Cattaneo, M. B., Marcucci, M., Vaivads, A., André, M., Khotyaintsev, Y., … Balogh, A. (2005). Cluster multispacecraft observations at the high-latitude duskside magnetopause: Implications for continuous and component magnetic reconnection. *Annales Geophysicae*, *23*(2), 461–473.

Russell, C. T., Anderson, B. J., Baumjohann, W., Bromund, K. R., Dearborn, D., Fischer, D., … Richter, I. (2016). The magnetospheric multiscale magnetometers. *Space Science Reviews*, *199*(1–4), 189–256. https://doi.org/10.1007/s11214-014-0057-3

Sonnerup, B. U. Ö., Paschmann, G., Papamastorakis, I., Sckopke, N., Haerendel, G., Bame, S. J., … Russell, C. T. (1981). Evidence for magnetic field reconnection at the Earth's magnetopause. *Journal of Geophysical Research*, *86*(A12), 10,049–10,067. https://doi.org/10.1029/JA086iA12p10049

Toledo-Redondo, S., André, M., Khotyaintsev, Y. V., Vaivads, A., Walsh, A., Li, W., … Russell, C. T. (2016). Cold ion demagnetization near the X-line of magnetic reconnection. *Geophysical Research Letters*, *43*, 6759–6767. https://doi.org/10.1002/2016GL069877

Toledo-Redondo, S., Vaivads, A., André, M., & Khotyaintsev, Y. V. (2015). Modification of the Hall physics in magnetic reconnection due to cold ions at the Earth's magnetopause. *Geophysical Research Letters*, *42*, 6146–6154. https://doi.org/10.1002/2015GL065129

Uchino, H., Kurita, S., Harada, Y., Machida, S., & Angelopoulos, V. (2017). Waves in the innermost open boundary layer formed by dayside magnetopause reconnection. *Journal of Geophysical Research: Space Physics*, *122*, 3291–3307. https://doi.org/10.1002/2016JA023300

Walsh, B. M., Phan, T. D., Sibeck, D. G., & Souza, V. M. (2014). The plasmaspheric plume and magnetopause reconnection. *Geophysical Research Letters*, *41*, 223–228. https://doi.org/10.1002/2013GL058802

Wang, S., Kistler, L. M., Mouikis, C. G., Liu, Y., & Genestreti, K. J. (2014). Hot magnetospheric O+ and cold ion behavior in magnetopause reconnection: Cluster observations. *Journal of Geophysical Research: Space Physics*, *119*, 9601–9623. https://doi.org/10.1002/2014JA020402

Wang, S., Kistler, L. M., Mouikis, C. G., & Petrinec, S. M. (2015). Dependence of the dayside magnetopause reconnection rate on local conditions. *Journal of Geophysical Research: Space Physics*, *120*, 6386–6408. https://doi.org/10.1002/2015JA021524

Yamada, M., Kulsrud, R., & Ji, H. (2010). Magnetic reconnection. *Reviews of Modern Physics*, *82*(1), 603–664. https://doi.org/10.1103/RevModPhys.82.603

Young, D. T., Burch, J. L., Gomez, R. G., De Los Santos, A., Miller, G. P., Wilson, P., … Webster, J. M. (2016). Hot plasma composition analyzer for the magnetospheric multiscale mission. *Space Science Reviews*, *199*(1), 407–470. https://doi.org/10.1007/s11214-014-0119-6